PAPER • OPEN ACCESS

The effect of the substrate on KF post deposition treatments of narrow gap Cu(In,Ga)Se_2 absorber layers

To cite this article: Jessica de Wild *et al* 2025 *J. Phys. Energy* **7** 045011

IOP Publishing J. Phys. Energy 7 (2025) 045011 https://doi.org/10.1088/2515-7655/adeae6

Journal of Physics: Energy

OPEN ACCESS

RECEIVED
8 May 2025

REVISED
23 June 2025

ACCEPTED FOR PUBLICATION
2 July 2025

PUBLISHED
5 August 2025

PAPER

The effect of the substrate on KF post deposition treatments of narrow gap Cu(In,Ga)Se_2 absorber layers

Jessica de Wild[1,2,3,*], **Guy Brammertz**[1,2,3], **Tim Oris**[1,2,3], **Tom Aernouts**[1,2,3] and **Bart Vermang**[1,2,3]

[1] Hasselt University, imo-imomec, Martelarenlaan 42, 3500 Hasselt, Belgium
[2] Imec, imo-imomec, Thor Park 8320, 3600 Genk, Belgium
[3] EnergyVille, imo-imomec, Thor Park 8320, 3600 Genk, Belgium
[*] Author to whom any correspondence should be addressed.

E-mail: Jessica.deWild@imec.be

Keywords: narrow band gap CIGS, alkali treatment, ToF-SIMS depth profiles, bias dependent admittance spectroscopy

Supplementary material for this article is available online

Abstract

Alkali post deposition treatments (PDT) are the standard method to increase the efficiency of Cu(In,Ga)Se_2 solar cells. In this study, the effects of potassium fluoride (KF) PDTs on narrow band gap Cu(In, Ga)Se_2 (CIS) layers are investigated. The CIS layers were grown on substrates such as glass with alkali-barrier/Mo, glass/Mo, and glass/indium-doped tin oxide. It was found that the effect of the PDT depends on the substrates and that there are conditions under which KF-PDT is detrimental to solar cell performance. Time-of-flight secondary ion mass spectrometry measurements revealed limited ion exchange between Na and K, which caused inhibited diffusion of K into the absorber layer. Further opto-electrical characterization indicated increased recombination in the solar cell. Capacitance–voltage–frequency measurements combined with modelling revealed the formation of an interface defect that is limiting the open circuit voltage and reducing the fill factor. Our findings suggest that the lack of K diffusion into the absorber layer promotes the formation of defects at the surface. This study highlights the complex interaction between alkali coming from PDT and the alkali already present in the absorber layer.

1. Introduction

The efficiency of Cu(In,Ga)Se_2 (CIGS) solar cells has steadily been increasing over the past decade and has reached an efficiency up the 23.6% [1]. Various engineering approaches have led to this efficiency, of which Ga gradients in the absorber layers, Na doping and alkali post deposition treatments (PDT) have been the most significant [2]. For the latest record solar cells heavier alkali treatments (Cs, Rb) have been implemented [1, 3]. This trend started in 2013, when K improved the efficiency drastically [4]. The beneficial effect is seen in the open circuit voltage (V_{OC}) and fill factor (FF).

More in-depth understanding of what the effect of the PDT is on the absorber layer and the front interface and how it improves efficiency is summarized in various reviews [2, 5]. In short, during the heat treatments and cooling down the heavier alkali ions replace the lighter alkali ions, which is known as the ion-exchange mechanism. The transport of ions is via grain boundaries and intragrain vacancies. During this exchange, Na is expelled from the grain interior to the grain boundaries, leaving copper vacancies behind, which increases the doping. At the front surface, K (Rb, Cs) reacts with Ga/In and expels Cu towards the interior. This results in a copper-poor front surface, or sometimes even a K–In–Se containing layer [6]. The copper-poor surface has a wider band gap due to lowering of the valence band, which is beneficial for rejecting holes. While alkali PDTs have been successfully implemented, there is still no clear understanding of the exact mechanisms behind the ion-exchange as they seem to depend more than solely on the copper vacancies. As such, relatively small variations of the absorber layer, such as the addition of Ag or S, require re-optimization of the processing parameters of the PDT. Sometimes the PDT reduces the performance, for instance, when S is added, the surface is copper rich, or back contact is adapted [7–10].

In this contribution, KF PDT have been performed on low band gap CI(G)S layers grown on various substrates. As the Ga is only at the back, we use CIS as an abbreviation. Narrow band gap CIS is being developed to be used in tandem cells as well as for bifacial applications. Since alkali treatments are a standard method to increase doping and improve absorber layer quality as well as interface properties, we implemented our previously developed KF-PDT [11] to these CIS absorber layers. It was found that the alkali-treatment is only beneficial when applied on substrates that have alkali barriers between glass and Mo. An alkali barrier means that the alkali content in the CIGS layers is externally controlled by adding it separately. When no alkali barrier is present, there is uncontrolled diffusion of the alkali from glass into the CIGS layer. To understand this phenomenon with respect to the various back contacts, we conducted Time of Flight Secondary Ion Mass Spectrometry (ToF-SIMS) measurements to find the alkali depth-profiles in the CIS absorber layer and the front interface with CdS. From these measurements it was concluded that there was limited exchange of Na with K when no alkali barrier was present. More in-depth opto-electrical characterization revealed the formation of defects at the CIS/CdS interface.

2. Experimental

The CIS layers were prepared on various substrates: glass/alkali-barrier/Mo, glass/Mo and glass/ITO. The ITO layers were annealed in air at 450 °C prior to CIS deposition. Na was either coming from glass or added by spin-coating [12]. Since ITO interacts with Na [13, 14], we also varied the amount of Na prior to CIS deposition by spin coating additional NaF. The different substrates are presented in table 1. Also, different glass substrates were used to investigate the effect of uncontrolled alkali coming from glass. The CIS layers were grown using a 3-stage co-evaporation process at 550 °C substrate temperature for all the steps. Only the first step contained Ga to have a back gradient. The final [Cu]/([Ga] + [In]) was ∼0.9 and [Ga]/([Ga] + [In]) (GGI) between 0.03 and 0.05. The samples on 3 mm glass had an additional 10 nm Ag layer deposited by evaporation on the Mo. The final CIS layers on Mo were about 2–2.4 μm thick and on ITO 1–1.2 μm.

After CIS deposition, the samples were transported in air to be finalized into solar cells. To remove oxides, ammonia sulphide treatment was done [15]. CdS buffer layers were deposited by chemical bath deposition. KF-PDTs are done as described in [11] using a cover. The samples with alkali PDT are presented in table 2. A molarity of 0.2 KF was previously the optimized concentration [11]. In this contribution we will present the results for 0.2 and 0.8 M KF. After CdS deposition, the samples were finalized by sputtered ZnO (50 nm) and ITO (150 nm). The solar cells on Mo with an area of 3 × 3 mm^2 were scribed by laser and the cells on ITO were scribed manually and had an approximate area of 3 × 3 mm^2.

The solar cells were measured with a Keithley 2400 source meter using four-point probes and Wavelabs Sinus 70 solar simulator. For the V_{OC}–J_{SC} measurements, the intensity varied from 0.3 sun to 1.3 sun. Bias-dependent admittance spectroscopy Capacitance–voltage–frequency (CVf) was performed using Agilent Precision LCR meter. The frequency varied from 1 kHz to 1 MHz using 31 logarithmically divided steps and the voltage varied from −1 to 1 V in 21 steps. The AC bias voltage was 30 mV. The analysis of the resulting CVf maps was done using the method described in [16].

Elemental depth profiles were measured using ToF-SIMS. ToF-SIMS measurements were performed with an ION.TOF NCS instrument (IONTOF GmBH, Muenster, Germany). Sputtering was conducted with a 2 keV O_2 ion beam. The sputter area of 350 × 350 μm^2 and an analysis area of 100 × 100 μm^2 were used for the depth profiles, with a raster of 128 × 128 pixels. Bi^+ (15 keV) was used as the analysis beam. For each run the current was kept the same between the samples and the depth profiles were normalized to the Mo signal (In signal in the case of ITO back contact). The comparison of ToF-SIMS data between samples of the same run was done without any corrections. When the samples were measured in different runs, corrections were made. This was applicable to the 2 mm sample when compared to the sample with alkali barrier and 3 mm glass, and the ITO sample with additional 0.4 M NaF when compared to the ITO and ITO 0.2 M NaF samples. The Mo signals of 2 mm glass was set to the same height as the Mo signals of the 3 mm and barrier glass substrates, and for the ITO 0.4 M NaF the In signal was set to the same height as the In signals from the ITO and ITO 0.2 M NaF substrates. The signal of the other ions was adapted accordingly, and the time scale was adapted as well. For the comparison between reference and KF-PDT samples on the same substrates, the sputter parameters were always the same as they were measured in the same run.

3. Results

3.1. The effect of the various substrates on solar cell performance

The importance of alkali, especially Na was discovered in the 90 s [17, 18]. Various studies showed that Na increased the doping and reduced recombination which led to the observed increase in V_{OC} and FF.

Table 1. Various substrates and Na sources for the CIS solar cells.

Sample	Na source
Barrier/Mo	0.2 M NaF
2 mm glass/Mo	Glass
3 mm glass/Mo/10 nm Ag	Glass
Glass/ITO	Glass
Glass/ITO	Glass + 0.2 M NaF
Glass/ITO	Glass + 0.4 M NaF

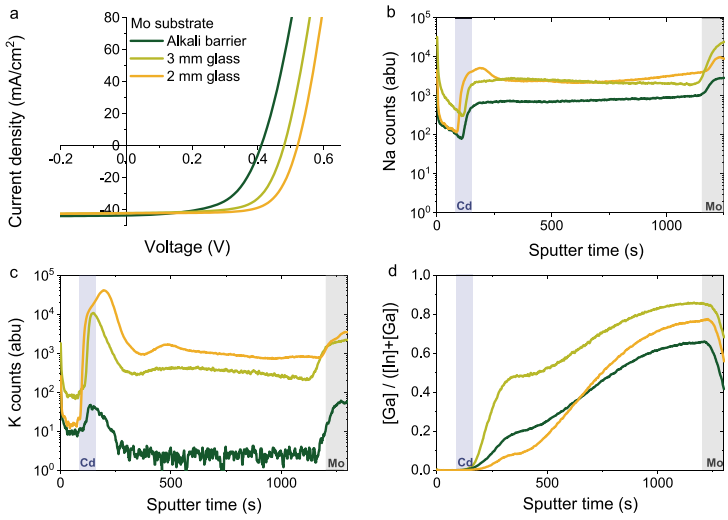

Figure 1. (a) J–V curves of solar cells with CIS layers grown on different Mo coated glass substrates with varying alkali sources (b) Na depth profiles of the different solar cells, (c) K depth profiles of the different solar cells, (d) GGI (ToF-SIMS counts) depth profiles of the various solar cells. Colour codes are presented in figure (a).

There was an optimum of the amount of Na though, which led to controlling the amount of Na [19]. Therefore, substrates with alkali barrier were used and Na was added before or after CIGS growth [20, 21]. The aim of this part of the study is to confirm and understand the effect (un)controlled Na (and K) coming from various substrates has in our samples. The effect of PDT is described in section 3.2

Table 1 summarizes the glass substrates that were used with the different back contacts and the Na sources. The amount of Na added by spin coating was based on previous experiments [12] and is not optimized for the thicker 3-stage CIS layers. K was always coming from the glass and is therefore not present in the samples grown on substrates with alkali barriers.

3.1.1. Solar cells on Mo coated glass substrates

CIS solar cells were prepared on different Mo substrates, presented in table 1. The current–voltage (J–V) curves of each sample with the highest V_{OC} are presented in figure 1(a). The V_{OC} varies significantly and increases from the CIS layer grown on the barrier glass to the 3 mm glass and 2 mm glass (statistical data can be found in the supplemental information S1). Since the growth process was the same for the all the samples, the difference comes from the substrates. Therefore, the alkali profiles are also measured. These are presented in figures 1(b) and (c) for Na and K respectively. The alkali profiles of the different glasses can be found in supplement S2 figure S2. We find that the variations in Na amount are small for the CIS layers grown on glass without barrier. In the bulk, the Na content is the same for these samples, but there seems to be a higher Na accumulation at the front of the CIS layer grown on 2 mm glass. The Na amount for the CIS layer grown on the barrier substrate, however, is almost a magnitude less than when Na is coming from glass. This likely indicates that the amount of added Na by spin coating can be higher, since the V_{OC} is also the lowest for this sample.

While the Na counts lie relatively close to each other, the K profiles reveal larger variations. Since the data is not calibrated, we do not know how the absolute K amount compares to the absolute Na amount, but we can discuss the difference between K profiles of the CIS samples. For the CIS layer grown on barrier glass, K is almost absent, which is expected as there was no K added. A significant amount of K is present in the CIS layers grown on the 3 and 2 mm glass substrates. Between these samples there is also a magnitude difference. These differences can be explained by the K content in the glass (see S2). Additionally, there is a steep

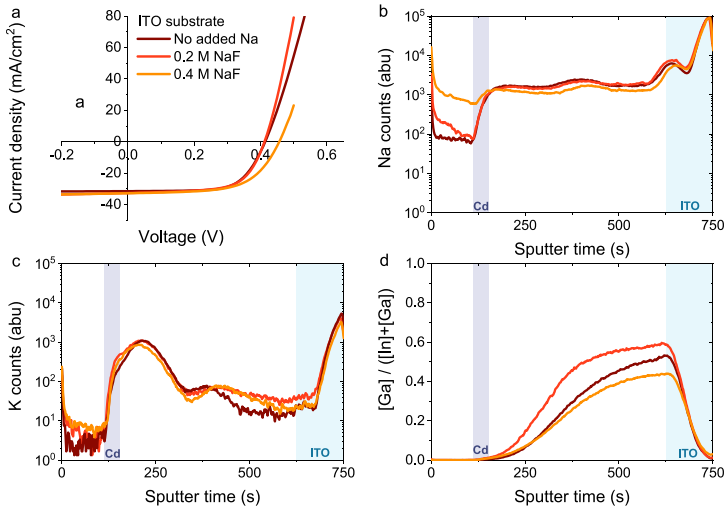

Figure 2. (a) J–V curves of solar cells with CIS layers grown on different ITO coated glass substrates with varying Na sources (b) NA depth profiles of the different solar, (c) K depth profiles of the different solar cells, (d) GGI (ToF-SIMS counts) depth profiles of the various solar cells. Colour codes are as presented in figure (a).

Table 2. KF-PDT of CIS layers on different substrates.

Sample	Alkali PDT
Barrier/Mo + 0.2 M NaF	0.2 KF
3 mm glass/ Mo/10 nm Ag	0.2 KF
3 mm glass/ Mo/10 nm Ag	0.8 KF
Glass/ITO + 0.4 M NaF	0.2 KF

increase of K at the front. This could partly be an artefact as the matrix changes from CIS to CdS/ZnO and alkali are very diffusive species, nevertheless it does indicate a significant amount of alkali at the front. Previously, such an accumulation at the front interface was thought to cause a barrier as a kink in the curve was observed [10]. That is not the case here since the CIS layer with the highest K counts at the front (2 mm glass) also gives the highest FF and V_{OC}. Thus, for these three samples on various substrates, it seems that more alkali resulted in better performance.

In figure 1(d) the GGI profiles are presented. What is presented here is the ToF-SIMS counts ratio, not the calibrated [Ga]/([Ga] + [In]) concentration. The differences in height of the GGI profiles come from variations in the Ga concentrations. The GGI measured by XRF varied between 3 and 5%, this is a factor two and likely explains the height differences. Besides the differences in height, the GGI slopes also vary between the samples. The steepest GGI slope is measured for the CIS layer grown on 2 mm glass. This also happens to be the sample with the best performance (12.7%) and highest alkali concentration. While the amount of alkali increases the V_{OC}, these variations in Ga profiles can also contribute to the changes in the solar cell parameters. In particular, the steepness of the slope (steepest for the 2 mm samples) can affect the recombination at the back contact and increase the V_{OC} [22]. The Ga profile is also dependent on the amount of Na in the absorber layer. It has been known for a while that In/Ga intermixing is inhibited in the presence of Na and that Ga accumulates at the back when more Na is present during growth [23]. Recently though, more detailed insights have been obtained, revealing a dependence of Ga/In intermixing on the Na/Cu ratio. When the ratio is low, but above a certain threshold, Ga/In intermixing is actually advanced resulting in less steep slopes [24, 25]. It is not unlikely that K has a similar influence on the Ga/In intermixing and contributes to the GGI slopes in our samples as well.

3.1.2. Solar cells on ITO coated glass substrates

CIS layers have also been prepared on ITO substrates with different Na amounts, see table 2. Figure 2(a) presents the *J–V* curves of the 3 different samples on ITO with increasing Na amount. We find that the V_{OC} and FF increase slightly with more Na (for statistical data, see S1). The alkali depth profiles are presented in figure 2(b) (Na) and (c) (K). Interestingly, there are no measurable changes in Na counts by adding more Na with spin coating. It is likely that the added amount is much lower compared to the Na coming from the glass. It may be noted, however, that the Na signal is higher at the front contacts (ZnO/ITO, between 0 and 125 counts). The K profiles are also the same; however, this is expected as there was no K added by spin coating

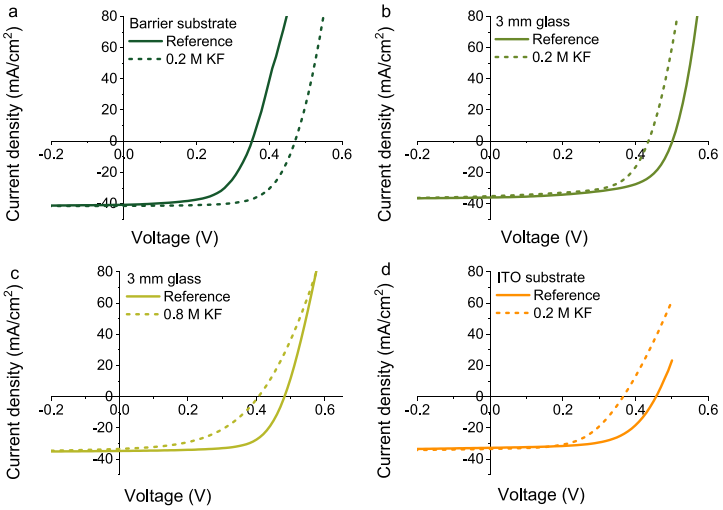

Figure 3. J–V curves of solar cells with (dashed) and without (solid) KF-PDT on CIS layers grown on different substrates. (a) barrier glass, (b) 3 mm glass + 10 nm Ag and low KF amount (c) 3 mm glass + 10 nm Ag and high KF amount, (d) ITO coated glass.

and K is only coming from the glass. In general, the K signal is lower than that of the 3 and 2 mm glass. This could indicate lower K diffusion through ITO compared to Mo. The K profiles show a steep decline from glass to absorber layer (figure S3). Additionally, there are no significant changes between the different GGI profiles of the ITO samples. Thus, the added Na does not significantly affect the GGI profile either. The GGI profiles differ compared to those of the CIS layer grown on Mo though. The CIS layers on Mo all have a flat plateau at the front (up to 500 s), while the CIS layers grown on ITO substrate have a GGI profile that is continuously decreasing towards the front. This could be due to the thinner CIS layer thickness but also lower amount of K. Nevertheless, the V_{OC} is higher with more initial Na. Unfortunately, we found that the ITO samples were not stable over time, and we were not able to investigate the cause for this increase in V_{OC}. The reason for the instability of the CIS solar cells grown on ITO back contact is yet to be investigated.

3.2. PDT

KF-PDTs were performed on the 3 mm glass with 10 nm Ag, ITO coated samples and the substrate with alkali barrier, see table 2. In figures 3(a)–(d) the *J–V* curves of these KF-PDT solar cells and their reference cells are presented. Statistical data from these measurements can be found in the S3 (V_{OC}) and S4 FF. We found that KF-PDT of the CIS layer grown on the substrate with alkali barrier was working as expected, improving V_{OC} and FF (figure 3(a)). Similar results were achieved in the past for CIGS solar cells [11, 12, 26]. The V_{OC} is still rather low, and we think that the KF-PDT cannot compensate for the initial low V_{OC} due to the low amount Na in the CIS layer that was added by spin coating prior to CIS layer growth. When similar alkali treatments are done on the CIS layers grown on the other two substrates, we find that the performance of the KF-PDT solar cells is worse than the references, see figures 3(b)–(d) (statistical data can be found in S3 and S4). A reason for this degradation could be that too little K was used, as a PDT with too little added heavy alkali may also reduce the performance [27]. However, increasing the amount of KF to 0.8 M, made the performance even worse, see figure 3(c). Similar results were also obtained using RbF, and the statistics of these results are also presented in supplements S3 and S4. We also find that the effect of the PDT on 3 mm glass is not dependent on Ag as for both KF as RbF PDT degradation is observed, see S5. To understand how a back contact can influence the PDT in such a way, we looked further into the alkali profiles using ToF-SIMS.

3.2.1. Alkali profiles upon KF-PDT

Alkali depth profiles of the solar cell presented in figure 3 were measured. The depth profiles of the solar cells that had KF-PDT are directly compared with their reference solar cells. The results are presented in figure 4. The top left graph (a) is from the CIS solar cell on barrier glass, which had a beneficial KF-PDT. We find that without KF-PDT there was a low amount of K in the samples, but a significant amount of Na (see also figures 1(b) and (c)). After KF-PDT the K signal is higher than the Na signal, and the Na signal is slightly lower than before (dashed lines). These results are consistent with our previous experiments on alkali PDT and similar trends have also been observed by other groups [4, 10, 11, 27, 28]. These results are interpreted as the ion-exchange mechanism where K (at least) partly replaces the Na in the absorber layer.

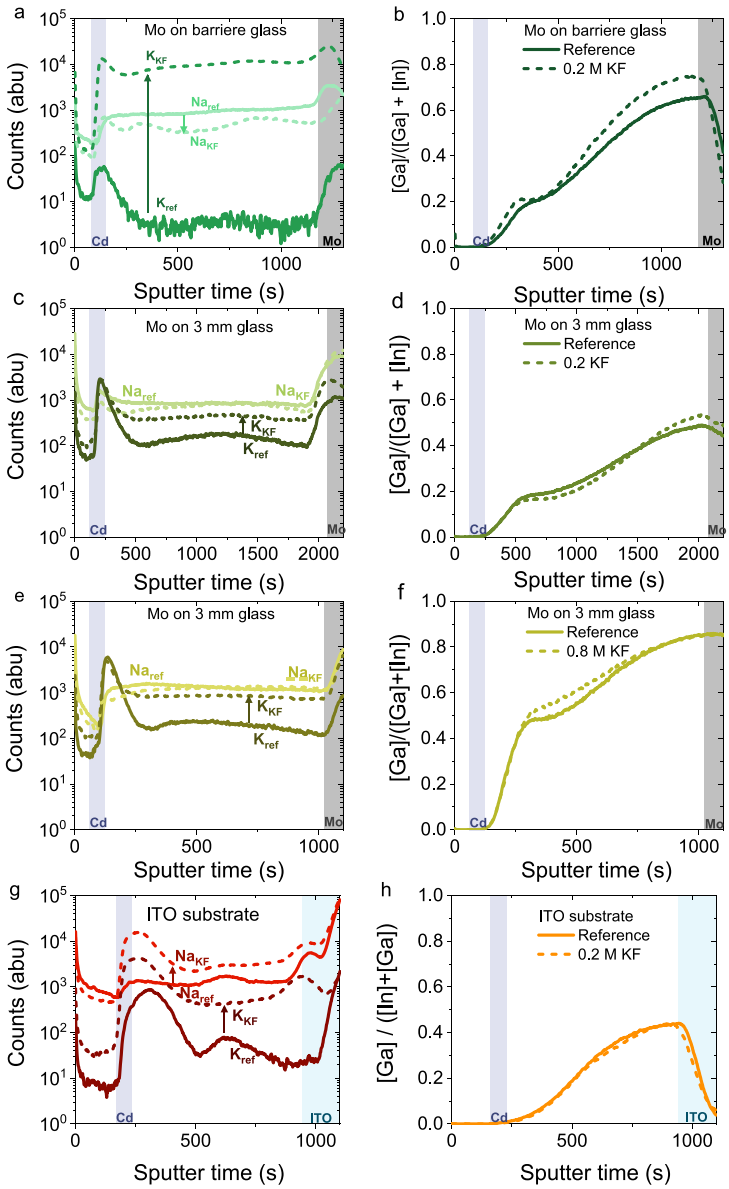

Figure 4. Alkali and GGI depth profiles of the different solar cells on the various substates with (dashed) and without (solid) KF-PDT (a) + (b) barrier glass, (c) + (d) 3 mm glass with low KF, (e) + (f) 3 mm glass with high KF, (g) + (f) ITO coated glass.

The alkali depth-profiles of the solar cells prepared on the substrates without alkali barrier reveal a different mechanism. Figure 4(c) presents the alkali profiles of the solar cells on 3 mm glass. Here, we find that the K signal is not higher than the Na signal after PDT and that the Na signal is not reduced. Even when more KF was added (figure 4(e)) we find that the K count is lower than the Na count before and after KF-PDT and that there is no change in Na signal. The solar cells on ITO substrates reveal even an increase in Na upon PDT (figure 4(g)). Also, the K signal remains below the Na signal after PDT. Since the opposite trend (figure 4(a)) is interpreted as the ion-exchange mechanism, we conclude that the trends in the other 3 samples are due to limited or no ion-exchange. Since the amount of added K is the same in all these samples, this limited exchange likely results in K remaining at the surface.

The right column of figure 4 presents the GGI profiles. We find no significant changes in the GGI profiles upon KF-PDT that could explain the difference between beneficial or detrimental KF-PDT. Thus, the only difference we find between beneficial and adverse effect of KF-PDT is related to the ion-exchange mechanism. Such an inhibited ion-exchange mechanism has been revealed to be detrimental in the case of a copper rich surface [9]. However, the lack of ion-exchange has been measured as well while having beneficial PDT [29].

3.2.2. Light intensity dependent J–V and C–V

Further electronic characterization such as light dependent *J–V* characterization and capacitance-voltage (*C–V*) measurements is performed on the different CIS layers grown on 3 mm glass. The data of the different

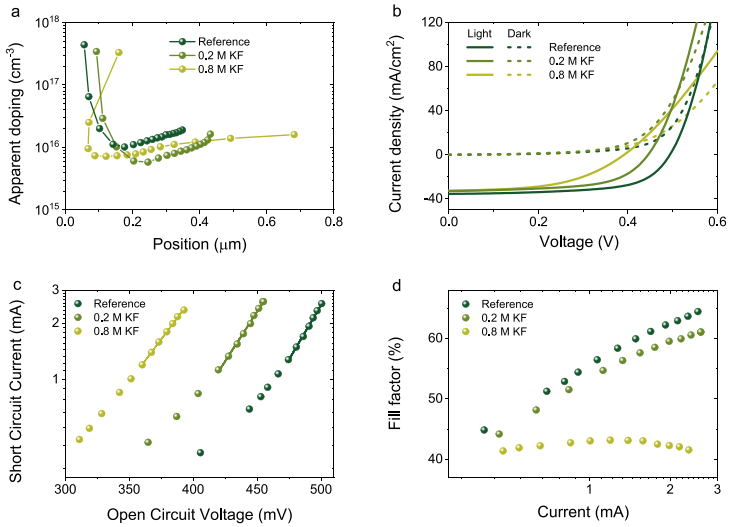

Figure 5. Opto-electrical measurements of the CIS solar cells grown on 3 mm glass without and with low and high KF. (a) apparent doping profile from C–V measurements at 100 kHz, (b) dark-light J–V curves, (c) J_{SC}–V_{OC} plot and fitting range for ideality factor, (d) FF vs J_{SC} plot.

measurements is presented in figure 5. Figure 5(a) presents the apparent doping profile of the different samples. It reveals that the doping slightly decreased upon KF treatment. One of the positive impacts of KF-PDT is the increase in net acceptor concentration, which is already not the case here. Since doping is a net result of alkali diffusion and copper vacancies, it also reveals the conflicting diffusion mechanisms during the PDT for these samples.

We also measured the dark *J–V* curves and overlaid them with the light curves; this is presented in figure 5(b). Thin film solar cells often have a cross-over which is attributed to voltage dependent current collection. It reduces the FF and V_{OC}. We find that this cross-over of the reference is at the highest voltage and shifting towards lower voltages for the 0.2 M KF and 0.8 M KF samples respectively. Explanations for the cross-over vary from the conduction band offset between CdS and CIGS interface, to the presence of defects in the bulk and buffer layer [30–33]. Shifts to lower voltages imply increased problems at the CI(G)S/CdS interface.

From the light dependent *J–V* curves, the ideality factor was calculated, using the relation between V_{OC} and I_{SC}: $V_{OC} = \frac{k_B T}{q} n(\ln\left(\frac{I_{SC}}{I_0} - 1\right)$, with n the ideality factor, T the temperature, I_0 the recombination current and k_B the Boltzmann constant. When V_{OC} and $\ln(J_{SC})$ are plotted against each other, the ideality factor can be determined from the slope $\frac{k_B T}{q} n$. This is presented in figure 5(c) A linear curve was fitted around 1 sun and the ideality factors of the different samples were calculated accordingly. We find an increase in the ideality factor from 1.44 to 1.58 and 1.84 for the reference, 0.2 M KF and 0.8 M KF samples respectively. A closer look also reveals that the curve is not linear over the full J_{SC} range for the reference and 0.2 M KF solar cells. This behaviour can be modelled using metastable defects in the bulk [34]. At last, the FF has also been plotted against the V_{OC}, see figure 5(d). As expected from the dark-light crossover, it does not increase linearly. The FF of the 0.8 M KF sample even appears to have a maximum. This can also be explained by metastable defects [34].

In summary, the current–voltage measurements indicate increased recombination, likely due to the presence of defects. This is in contrast to what is often found when the PDT is detrimental. Barriers are general the culprit in these cases. However, the *J–V* curves presented here reveal no kinks or s-shapes, which are often present with barriers [8, 10]. To find what kind of defects are formed and where in the stack, CVf measurements are performed.

3.2.3. CVf measurements and modelling

CVf measurements were performed on the 3 samples. With this method, the data obtained from bias dependence admittance spectroscopy are visualized in a 2D map. The results are presented in figure 6. The left column presents the measurements and the right column the modelled maps. In [16] a more detailed explanation of the method and the various features that can be found in these maps are described. For instance, the light pink area at high voltage and low frequency in all the measured maps can be attributed to dissipation. The dissipation factor $D = G/(2\pi fC)$, with G the conductance, f the frequency and C the capacitance, is then too large and the capacitance is not correctly measured. The yellowish feature at the top

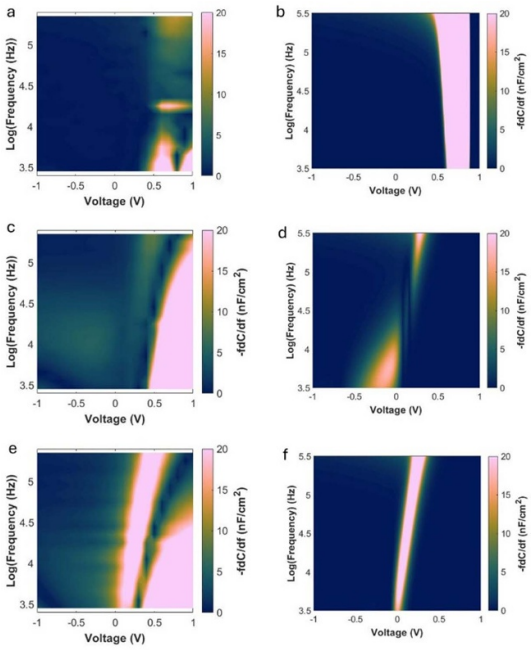

Figure 6. Measured and modelled CVf maps of the 3 CIS cells on 3 mm glass without KF PDT (a) and (b) and with low (c) and (d) and high KF (e) and (f).

right visible in map a) is tentatively attributed to a CdS/CIGS interface defect and limiting the V_{OC} [35]. Note that the scales are the same for all the measured and modelled CVf maps.

Since the features at higher voltages are difficult to interpret due to high dissipation, we will look at the features visible below 0.5 V. In this range we find large differences between the 3 samples. The map of the reference solar cell (6(a)) is completely dark blue implying that there are no electronic losses in this frequency and bias range. The map of the 0.2 M KF sample (6(c)) shows a lighter greenish area at negative voltage around 10 kHz and a yellow/greenish feature at the top around 0.4 V. The CVf map of the 0.8 M KF sample (6(e)) reveals a sharp light pink feature going from 0.4 V for high frequencies to 0 V for low frequencies. To understand what these features mean, the maps are modelled as described in [16].

For modelling the CVf maps, SCAPS simulation software has been used [36, 37]. Standard parameters for the various layers where applied [22], with slight adaptation for the low band gap of CIS by increasing the electron affinity of the CIS layer to 4.5 eV and lowering the band gap to 1 eV. The parameters can be found in S6. The sharp features seen in map 6(e) could be modelled using an interface defect. This is presented in figure 6(f). Interestingly, when going to a lower concentration of the same interface defect, the red feature splits into two parts, which is presented in figure 6(d). This is quite similar to what is presented in map 6(c). It is thus likely that the 2 maps of 0.2 M KF and 0.8 M KF present the same interface defects but with different concentrations. When we remove the interface defect, we get a dark blue map (b) but with a large feature at higher bias voltage >0.5 V. From the CVf measurements and the modelling, it seems that the samples that have deteriorated performance after KF-PDT suffer from an interface defect. This defect increases in concentration when more initial K is added and moves to higher voltages (>0.5 V) when there is no KF treatment.

4. Conclusion and discussion

In this study, KF PDT have been performed on low band gap CIS layers grown on different substrates. The performance of the CIS solar cells grown on various substrates varied between 10% and 13%. We could relate these variations in performance to change in the Ga profile at the back and the amount of alkali present during growth. We found a clear trend of increased alkali concentration (K and Na) with increased performance. These results are consistent with the standard theories on the effect alkali has on the performance.

When PDT was performed, we found both beneficial as well as detrimental effects upon the KF-PDT. To better understand what was happening, ToF-SIMS depth profiles have been measured of CIS cells with and without KF-PDT. When KF-PDT was performed there was a clear difference between the changes in depth profiles of cells that had beneficial KF-PDT and the cells that had deteriorated KF-PDT. While beneficial

KF-PDT reveals exchange between Na and K, known as ion-exchange mechanisms, the K counts remain low for the detrimental KF-PDT which is explained as inhibited ion-exchange mechanism. It is hypothesized that K does not diffuse into the absorber layer and remains on the surface during the heat treatment.

The *J*–*V* characteristics and *C*–*V* measurements revealed clear trends from the reference towards higher amounts of initial KF. Those trends were as follows: (a) small reduction in net doping concentration, (b) increase in ideality factor, and (c) dark-light cross-over to lower voltages. These are indicative signs that the cells are limited by increased recombination. The CVf maps revealed distinguishable features that could be modelled by an acceptor defect at the CIS/CdS interface. It has to be noted that similar features can be modelled by a bulk defect very close to the interface as well. It nevertheless points to problems near the interface. We hypothesized that the lack of K diffusion into the absorber layer induces this interface defect and limits the performance.

There are only limited studies on deteriorated performance after PDT. Circumstances that reveal adverse effect of PDT are as follows: Ag addition [7], sulfurized CIGSSe [8], copper rich surface [9], AlOx passivization layer at the back [10], too low annealing temperature [38], and anneal using sequentially grown CIGS [39]. Often when too much or too little heavy alkali is added, deterioration is observed as well [27, 40, 41]. In this contribution we show that changes in substrates can alter the PDT as well.

It should be noted that this is not a common observation, as many groups perform alkali PDT on glass substrates without a barrier. However, many groups conduct the PDT *in-situ*, without air exposure or cooling down. Therefore, it is likely that the process—KF deposition at room temperature (RT), followed by annealing at higher temperatures—is detrimental to samples on non-barrier substrates but not on barrier substrates. One theory is that KF deposition at RT is problematic if the surface is already saturated with alkali, which is likely the case for the CIS layer grown on glass without alkali barrier. It is known that alkali move around during the cooling down and annealing steps, resulting in a redistribution of the alkali [42, 43]. The fact that the processing window varies for each sample and alkali used (K, Rb, Cs), indicates that the interaction between alkali in the absorber layer and those added by PDT is still not fully understood. Thus, a greater understanding of this interaction will lead to a more targeted implementation of heavier alkali PDT for the various CIGS absorber layers.

Data availability statement

All data that support the findings of this study are included within the article (and any supplementary files).

Acknowledgments

This work has received funding from the European Union's Horizon Europe research and innovation programme under Grant Agreement No. 101075626 (SITA-project) and from the Flemish government for FWO research Project G0A1623N (ENGAGED). We also acknowledge TNO facility in Einhoven NL for the use of the co-evaporation tool.

Author contributions

Jessica de Wild 0000-0003-2291-4674
Conceptualization (lead), Data curation (lead), Formal analysis (lead), Funding acquisition (equal), Investigation (lead), Methodology (lead), Project administration (lead), Validation (lead), Visualization (lead), Writing – original draft (lead), Writing – review & editing (equal)

Guy Brammertz 0000-0003-1404-7339
Conceptualization (supporting), Formal analysis (supporting), Methodology (supporting)

Tim Oris 0000-0003-0007-4918
Resources (supporting), Writing – review & editing (supporting)

Tom Aernouts 0000-0002-3004-6080
Resources (equal), Writing – review & editing (equal)

Bart Vermang 0000-0003-2669-2087
Funding acquisition (equal), Project administration (equal), Resources (equal), Supervision (supporting)

References

[1] Keller J, Kiselman K, Donzel-Gargand O, Martin N M, Babucci M, Lundberg O, Wallin E, Stolt L and Edoff M 2024 High-concentration silver alloying and steep back-contact gallium grading enabling copper indium gallium selenide solar cell with 23.6% efficiency *Nat. Energy* **9** 1–12

[2] Zhao C *et al* 2023 Advances in CIGS thin film solar cells with emphasis on the alkali element post-deposition treatment *Mater. Rep.* **3** 100214

[3] Nakamura M, Yamaguchi K, Kimoto Y, Yasaki Y, Kato T and Sugimoto H 2019 Cd-free Cu(In,Ga)(Se,S)$_2$ thin-film solar cell with record efficiency of 23.35% *IEEE J. Photovolt.* **9** 1863–7

[4] Chirilă A *et al* 2013 Potassium-induced surface modification of Cu(In,Ga)Se$_2$ thin films for high-efficiency solar cells *Nat. Mater.* **12** 1107–11

[5] Siebentritt S *et al* 2020 Heavy alkali treatment of Cu(In,Ga)Se$_2$ solar cells: surface versus bulk effects *Adv. Energy Mater.* **10** 1903752

[6] Reinhard P *et al* 2015 Features of KF and NaF postdeposition treatments of Cu(In,Ga)Se$_2$ absorbers for high efficiency thin film solar cells *Chem. Mater.* **27** 5755–64

[7] Valdes N H, Jones K J, Opila R L and Shafarman W N 2019 Influence of Ga and Ag on the KF treatment chemistry for CIGS solar cells *IEEE J. Photovolt.* **9** 1846–51

[8] Keller J, Bilousov O V, Neerken J, Wallin E, Martin N M, Riekehr L, Edoff M and Platzer-Björkman C 2020 Heavy alkali treatment of post-sulfurized Cu(In,Ga)Se$_2$ layers: effect on absorber properties and solar cell performance *Sol. RRL* **4** 2000248

[9] Lepetit T, Harel S, Arzel L, Ouvrard G and Barreau N 2017 KF post deposition treatment in co-evaporated Cu(In,Ga)Se$_2$ thin film solar cells: beneficial or detrimental effect induced by the absorber characteristics *Prog. Photovolt.* **25** 1068–76

[10] de Wild J, Birant G, Thiruvallur Eachambadi R, Kohl T, Buldu D G, Brammertz G, Manca J V, Meuris M, Poortmans J and Vermang B 2021 Detrimental impact of Na upon Rb postdeposition treatments of Cu(In,Ga)Se$_2$ absorber layers *Sol. RRL* **5** 2170094

[11] de Wild J, Buldu D G, Schnabel T, Simor M, Kohl T, Birant G, Brammertz G, Meuris M, Poortmans J and Vermang B 2019 High V_{oc} upon KF post-deposition treatment for ultrathin single-stage coevaporated Cu(In, Ga)Se$_2$ solar cells *ACS Appl. Energy Mater.* **2** 6102–11

[12] de Wild J, Simor M, Buldu D G, Kohl T, Brammertz G, Meuris M, Poortmans J and Vermang B 2019 Alkali treatment for single-stage co-evaporated thin $CuIn_{0.7}Ga_{0.3}Se_2$ solar cells *Thin Solid Films* **671** 44–48

[13] Son Y-S, Yu H, Park J-K, Kim W M, Ahn S-Y, Choi W, Kim D and Jeong J 2019 Control of structural and electrical properties of indium tin oxide (ITO)/Cu(In,Ga)Se$_2$ interface for transparent back-contact applications *J. Phys. Chem. C* **123** 1635–44

[14] Li Y, Yin G and Schmid M 2022 Bifacial semi-transparent ultra-thin Cu(In,Ga)Se$_2$ solar cells on ITO substrate: how ITO thickness and Na doping influence the performance *Sol. Energy Mater. Sol. Cells* **234** 111431

[15] Buffière M, Mel A-A E, Lenaers N, Brammertz G, Zaghi A E, Meuris M and Poortmans J 2015 Surface cleaning and passivation using $(NH_4)_2S$ treatment for Cu(In,Ga)Se$_2$ solar cells: a safe alternative to KCN *Adv. Energy Mater.* **5** 1401689

[16] Brammertz G, Kohl T, de Wild J, Buldu D G, Birant G, Meuris M, Poortmans J and Vermang B 2020 Bias-dependent admittance spectroscopy of thin-film solar cells: experiment and simulation *IEEE J. Photovolt.* **10** 1102–11

[17] Hedstrom J, Ohlsen H, Bodegard M, Kylner A, Stolt L, Hariskos D, Ruckh M and Schock H-W 1993 ZnO/CdS/Cu(In,Ga)Se$_2$ thin film solar cells with improved performance *Conf. Record Twenty Third IEEE Photovoltaic Specialists Conf.—1993 (Cat. No. 93CH3283-9)* pp 364–71

[18] Holz J, Karg F and Philipsborn H V 1994 The effect of substrate impurities on the electronic conductivity in CIS thin films *Proc. 12th European Photovoltaic Solar Energy Conf.* pp 1592–5

[19] Karami A, Morawski M, Kempa H, Scheer R and Cojocaru-Mirédin O 2024 Sodium in Cu(In, Ga)Se$_2$ solar cells: to be or not to be beneficial *Sol. RRL* **8** 2300544

[20] Rudmann D, da Cunha A F, Kaelin M, Kurdesau F, Zogg H, Tiwari A N and Bilger G 2004 Efficiency enhancement of Cu(In,Ga)Se$_2$ solar cells due to post-deposition Na incorporation *Appl. Phys. Lett.* **84** 1129–31

[21] Salomé P M P, Rodriguez-Alvarez H and Sadewasser S 2015 Incorporation of alkali metals in chalcogenide solar cells *Sol. Energy Mater. Sol. Cells* **143** 9–20

[22] Frisk C, Platzer-Björkman C, Olsson J, Szaniawski P, Wätjen J T, Fjällström V, Salomé P and Edoff M 2014 Optimizing Ga-profiles for highly efficient Cu(In, Ga)Se$_2$ thin film solar cells in simple and complex defect models *J. Phys. D: Appl. Phys.* **47** 485104

[23] Lundberg O, Lu J, Rockett A, Edoff M and Stolt L 2003 Diffusion of indium and gallium in Cu(In,Ga)Se$_2$ thin film solar cells *J. Phys. Chem. Solids* **64** 1499–504

[24] Colombara D 2019 Frank-Turnbull dopant migration may enhance heteroatom diffusivity: evidence from alkali-doped Cu(In,Ga)Se$_2$ *Phys. Rev. Mater.* **3** 054602

[25] Colombara D, Conley K, Malitckaya M, Komsa H-P and Puska M J 2020 The fox and the hound: in-depth and in-grain Na doping and Ga grading in Cu(In,Ga)Se$_2$ solar cells *J. Mater. Chem. A* **8** 6471–9

[26] de Wild J, Kohl T, Buldu D G, Birant G, Parragh D M, Brammertz G, Meuris M, Poortmans J and Vermang B 2020 KF postdeposition treatment in N_2 of single-stage thin Cu(In,Ga)Se$_2$ absorber layers *IEEE J. Photovolt.* **10** 255–8

[27] Feurer T, Fu F, Weiss T P, Avancini E, Löckinger J, Buecheler S and Tiwari A N 2019 RbF post deposition treatment for narrow bandgap Cu(In,Ga)Se$_2$ solar cells *Thin Solid Films* **670** 34–40

[28] Jackson P, Wuerz R, Hariskos D, Lotter E, Witte W and Powalla M 2016 Effects of heavy alkali elements in Cu(In,Ga)Se$_2$ solar cells with efficiencies up to 22.6% *Phys. Status Solidi (RRL)* **10** 583–6

[29] Khatri I, Fukai H, Yamaguchi H, Sugiyama M and Nakada T 2016 Effect of potassium fluoride post-deposition treatment on Cu(In,Ga)Se$_2$ thin films and solar cells fabricated onto sodalime glass substrates *Sol. Energy Mater. Sol. Cells* **155** 280–7

[30] Gloeckler M, Jenkins C R and Sites J R 2002 Explanation of light/dark superposition failure in CIGS solar cells *MRS Online Proc. Library* vol 763 p 522

[31] Yang S, Khelifi S, de Wild J, Vermang B and Lauwaert J 2021 Investigation of recombination mechanisms in Cu(In,Ga)Se solar cells using numerical modelling *Sol. Energy* **228** 464–73

[32] Eisgruber I L, Granata J E, Sites J R, Hou J and Kessler J 1998 Blue-photon modification of nonstandard diode barrier in CuInSe$_2$ solar cells *Sol. Energy Mater. Sol. Cells* **53** 367–77

[33] Niemegeers A, Burgelman M, Herberholz R, Rau U, Hariskos D and Schock H-W 1998 Model for electronic transport in Cu(In,Ga)Se$_2$ solar cells *Prog. Photovolt.* **6** 407–21

[34] Weiss T P, Ramírez O, Paetel S, Witte W, Nishinaga J, Feurer T and Siebentritt S 2023 Metastable defects decrease the fill factor of solar cells *Phys. Rev. Appl.* **19** 024052

[35] Brammertz G *et al* 2025 Investigation of recombination mechanisms in electronic devices using bias-dependent admittance spectroscopy applied to CIGS solar cells *ACS Appl. Mater. Interfaces* submitted
[36] Burgelman M, Decock K, Khelifi S and Abass A 2013 Advanced electrical simulation of thin film solar cells *Thin Solid Films* **535** 296–301
[37] Decock K, Zabierowski P and Burgelman M 2012 Modeling metastabilities in chalcopyrite-based thin film solar cells *J. Appl. Phys.* **111** 043703
[38] Eslam A, Wuerz R, Hauschild D, Weinhardt L, Hempel W, Powalla M and Heske C 2021 Impact of substrate temperature during NaF and KF post-deposition treatments on chemical and optoelectronic properties of alkali-free Cu(In,Ga)Se_2 thin film solar cell absorbers *Thin Solid Films* **739** 138979
[39] Zheng X, Xie C, Li W, Aberle A G and Venkataraj S 2020 Investigations of potassium-induced surface treatment of Cu(In,Ga)Se_2 (CIGSe) thin film solar cells prepared by two-stage process using elemental selenium *Appl. Surf. Sci.* **525** 146368
[40] Zahedi-Azad S, Maiberg M and Scheer R 2020 Effect of Na-PDT and KF-PDT on the photovoltaic performance of wide bandgap Cu (In,Ga)Se_2 solar cells *Prog. Photovolt.* **28** 1146–57
[41] Chen Y-H, Kuo R-T, Lin W-C, Lai C-Y and Lin T-Y 2024 Cesium modulation in Cu(In, Ga)(S, $Se)_2$ solar cells: comprehensive analysis on interface, surface, and grain boundary *ACS Appl. Mater. Interfaces* **16** 32220–31
[42] Kamikawa Y, Nishinaga J, Ishizuka S, Tayagaki T, Guthrey H, Shibata H, Matsubara K and Niki S 2018 Effect of thermal annealing on the redistribution of alkali metals in Cu(In,Ga)Se_2 solar cells on glass substrate *J. Appl. Phys.* **123** 093101
[43] Cheng S, Sun Y and Liu H 2025 Introduction of the distribution of Cs in Cu(In,Ga)Se_2 photovoltaic absorbers following post-deposition treatment with CsF *J. Meas. Eng.* **13** 35–41